IceCube

Thomas Gaisser[1] and Francis Halzen[2]

[1]Bartol Research Institute and Department of Physics and Astronomy, University of Delaware, Newark, Delaware 19716

[2]Department of Physics, University of Wisconsin–Madison, Madison, Wisconsin 53703

Annu. Rev. Nucl. Part. Sci. 2014. 64:101–23

First published online as a Review in Advance on June 19, 2014

The *Annual Review of Nuclear and Particle Science* is online at nucl.annualreviews.org

This article's doi: 10.1146/annurev-nucl-102313-025321

Keywords

neutrino astronomy, cosmic rays, dark matter, neutrino properties

Abstract

IceCube is the first kilometer-scale neutrino detector. Built primarily for neutrino astronomy, it has recently discovered events with energies above 100 TeV that are likely to be from distant sources beyond the solar system. Among the events are three with deposited energies of more than 1 PeV, the highest-energy neutrinos ever detected. We review the astrophysical arguments that motivate such a large detector, and we describe how it works and how the high-energy events are reconstructed and identified above the background of atmospheric neutrinos. We also describe the broad range of neutrino physics and particle astrophysics topics addressed by IceCube, as well as its potential for the future.

Contents

1. INTRODUCTION

Soon after the 1956 observation of the neutrino (1), the idea emerged that it represented the ideal astronomical messenger (2–4). The concept has since been demonstrated: Neutrino detectors have "seen" the Sun and detected a supernova in the Large Magellanic Cloud in 1987. Both observations were of tremendous importance; the former showed that neutrinos have a tiny mass, opening the first chink in the armor of the Standard Model of particle physics, and the latter confirmed the basic nuclear physics of the death of stars.

High-energy neutrinos have distinct potential to probe the extreme Universe. Neutrinos reach us from the edge of the Universe without absorption and with no deflection by magnetic fields. They can escape unscathed from the inner neighborhood of black holes and from the accelerators in which cosmic rays are born. Their weak interactions also make neutrinos very difficult to detect. Immense particle detectors are required to collect cosmic neutrinos in statistically significant numbers (5). By the 1970s, researchers had already understood (6) that a kilometer-scale detector was needed to observe the "cosmogenic" neutrinos produced in the interactions of cosmic rays with background microwave photons (7).

Above a threshold of $\sim 4 \times 10^{19}$ eV, cosmic rays interact with the microwave background, introducing an absorption feature in the cosmic-ray flux, the Greisen–Zatsepin–Kuzmin (GZK) cutoff (8, 9). The mean free path of extragalactic cosmic rays propagating in the microwave background is limited to <100 Mpc. Therefore, secondary neutrinos produced in these interactions are the only probe of the still-enigmatic sources at further distances. Realistic calculations (10) of the neutrino flux associated with the observed flux of extragalactic cosmic rays appeared in the 1970s and predicted on the order of one event per year in a kilometer-scale detector, subject to astrophysical uncertainties. Today's estimates of the sensitivity for observing potential cosmic-ray accelerators such as galactic supernova remnants (SNRs), active galactic nuclei (AGN), and γ-ray bursts (GRBs) unfortunately point to the same extreme requirement (5). Building a neutrino telescope has been a daunting technical challenge.

Given a detector's required size, early efforts concentrated on instrumenting large volumes of natural water with photomultipliers that detect the Cherenkov light emitted by the secondary

particles produced when neutrinos interact with nuclei inside or near the detector (11). After a two-decade-long effort, building the Deep Underwater Muon and Neutrino Detector (DUMAND) in the sea off the main island of Hawaii unfortunately failed (12). However, DUMAND pioneered many of the detector technologies in use today and inspired the deployment of a smaller instrument in Lake Baikal (13), as well as efforts to commission neutrino telescopes in the Mediterranean (14–16). These have paved the way toward the planned construction of KM3NeT (16).

The first telescope on the scale envisaged by the DUMAND Collaboration was realized instead by transforming a large volume of deep Antarctic ice into a particle detector, the Antarctic Muon and Neutrino Detector Array (AMANDA). In operation from 2000 to 2009 (17), AMANDA represented the proof of concept for the kilometer-scale neutrino observatory IceCube (18, 19), completed in 2010 (**Figure 1**). We write this review at the critical time when IceCube data taken with the completed detector have revealed the first evidence for a flux of high-energy neutrinos reaching us from beyond the solar system (20).

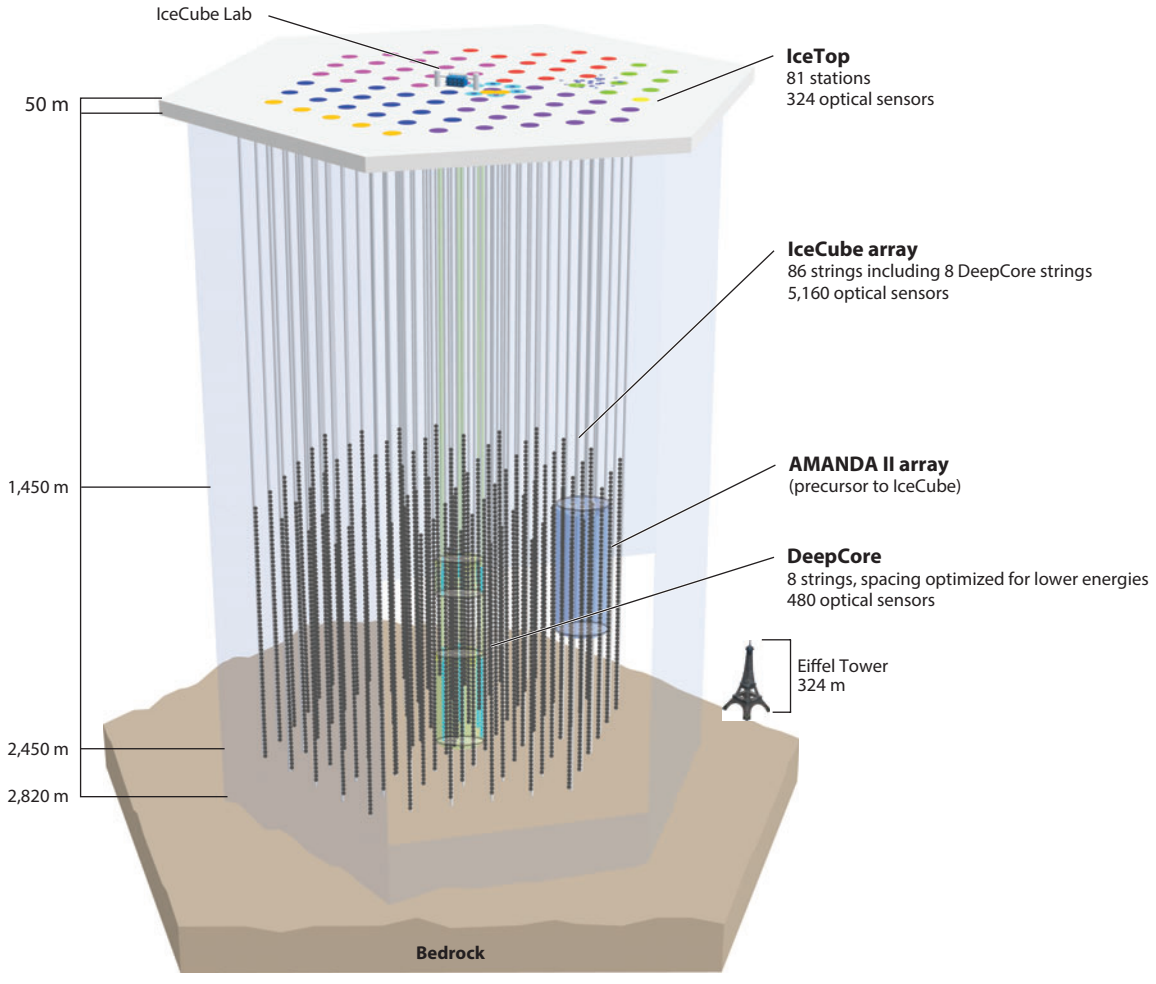

Figure 1

Artist's drawing of IceCube at the National Science Foundation's Amundsen–Scott South Pole Station. The former AMANDA detector is shown in blue and the DeepCore subarray in green.

2. RATIONALE FOR THE CONSTRUCTION OF KILOMETER-SCALE NEUTRINO DETECTORS

The construction of kilometer-scale neutrino detectors is motivated primarily by the prospect of detecting neutrinos associated with the sources of high-energy cosmic rays. Cosmic-ray accelerators produce particles with energies in excess of 100 EeV; we still do not know where or how (21). The bulk of the cosmic rays are Galactic in origin. Any association with our Galaxy presumably disappears at EeV energy, when the gyroradius of a proton in the Galactic magnetic field exceeds its size. The cosmic-ray spectrum exhibits a rich structure above an energy of ~0.1 EeV, but where exactly the transition to extragalactic cosmic rays occurs is a matter of debate.

The detailed blueprint for a cosmic-ray accelerator must meet two challenges: The highest-energy particles in the beam must reach beyond 10^3 TeV (10^8 TeV) for Galactic (extragalactic) sources, and their luminosities must be able to accommodate the observed flux. Both requirements represent severe constraints that have guided theoretical speculations.

SNRs were proposed as a likely source of cosmic rays as early as 1934 by Baade & Zwicky (22). Notably, they assumed the sources were extragalactic because the most recent supernova in the Milky Way dates to 1572. After diffusion in the interstellar medium was understood, supernova explosions in the Milky Way became the source of choice for the origin of Galactic cosmic rays (23), although after 50 years the issue is still being debated (24). The idea is widely accepted because of energetics. Three Galactic supernova explosions per century converting a reasonable fraction of a solar mass into particle acceleration can accommodate the steady flux of cosmic rays in the Galaxy.

Energetics also guides speculations on the origin of extragalactic cosmic rays. By integrating the cosmic-ray spectrum above the ankle at ~4 EeV, it is possible to estimate the energy density in extragalactic cosmic rays as $\sim 3 \times 10^{-19}$ erg cm^{-3} (25). This value is rather uncertain because of our ignorance of the precise energy where the transition from Galactic to extragalactic sources occurs. The power required for a population of sources to generate this energy density over the Hubble time of 10^{10} years is 2×10^{37} erg s^{-1} Mpc^{-3}. A GRB fireball converts a fraction of a solar mass into the acceleration of electrons, observed as synchrotron photons. The observed energy in extragalactic cosmic rays can be accommodated with the reasonable assumption that shocks in the expanding GRB fireball convert roughly equal energy into the acceleration of electrons and cosmic rays (26). It so happens that 2×10^{51} erg per GRB will yield the observed energy density in cosmic rays after 10^{10} years, given that their rate is on the order of 300 Gpc^{-3} year^{-1}. Hundreds of bursts per year over a Hubble time produce the observed cosmic-ray density, just as three supernovae per century accommodate the steady flux in the Galaxy.

Problem solved? Not really: It turns out that the same result can be achieved assuming that AGN convert, on average, 2×10^{44} erg s^{-1} each into particle acceleration (27). As is the case for GRBs, this is an amount that matches the AGN output in electromagnetic radiation. Whether GRBs or AGN, the observation that cosmic-ray accelerators radiate similar energies in photons and cosmic rays may not be an accident.

Neutrinos will be produced at some level in association with the cosmic-ray beam. Cosmic rays accelerated in regions of high magnetic fields near black holes or neutron stars inevitably interact with radiation surrounding them. Thus, cosmic-ray accelerators are beam dumps. Cosmic rays accelerated in supernova shocks interact with gas in the Galactic disk, producing equal numbers of pions of all three charges that decay into pionic photons and neutrinos. A larger source of secondaries is likely to be gas near the sources, for example, cosmic rays interacting with high-density molecular clouds that are ubiquitous in the star-forming regions where supernovae are more likely to explode. For extragalactic sources, the neutrino-producing target may be electromagnetic, for

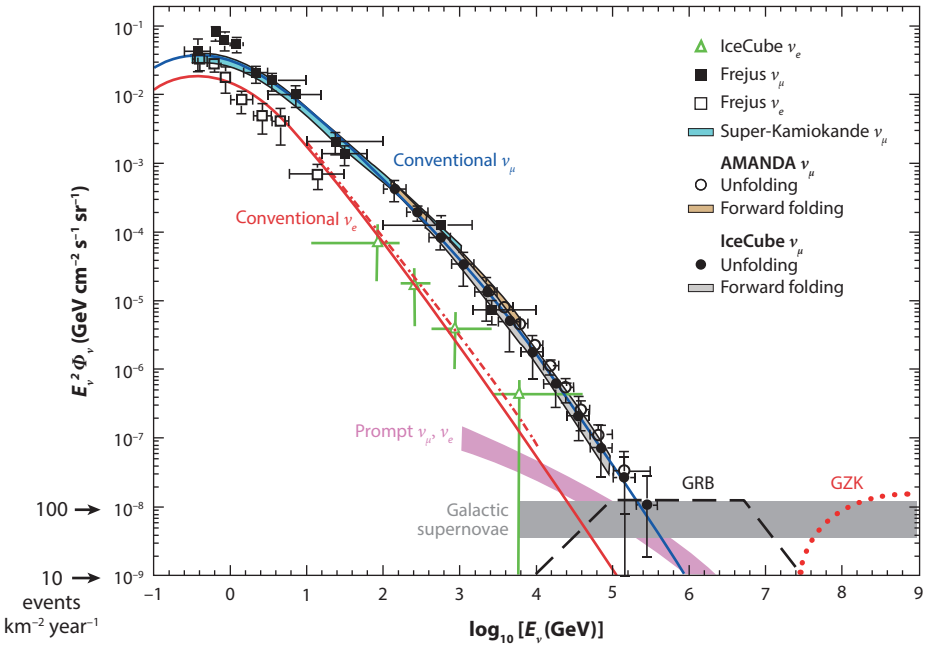

Figure 2

Anticipated astrophysical neutrino fluxes are compared with measured and calculated fluxes of atmospheric neutrinos. The shaded band indicates the level of model-dependent expectations for high-energy neutrinos of astrophysical origin. Measurements of ν_μ from Super-Kamiokande (28), Frejus (29), AMANDA (30, 31), and IceCube (32, 33) are shown along with the ν_e spectrum at high energy (*green open triangles*) (34). Calculations of conventional ν_e (*red line*) and ν_μ (*blue line*) (35), ν_e (*red dotted line*) (36), and charm-induced neutrinos (*magenta band*) (37) are also shown. Abbreviations: GRB, γ-ray burst; GZK, Greisen–Zatsepin–Kuzmin cutoff.

instance, photons radiated by the accretion disk of an AGN, or synchrotron photons that coexist with protons in the expanding fireball producing a GRB. **Figure 2** compares estimates of astrophysical neutrino fluxes with measurements of atmospheric neutrinos. The estimates, discussed briefly in the following paragraphs, set the level at

$$E_\nu^2 \frac{dN_\nu}{dE_\nu} \simeq 10^{-8}\,\mathrm{GeV\,cm^{-2}\,s^{-1}\,sr^{-1}} \qquad 1.$$

per flavor, or somewhat less.

Estimating the neutrino flux associated with cosmic rays accelerated in SNRs and GRBs is relatively straightforward because both the beam, identified with the observed cosmic-ray flux, and the targets, observed by astronomers, are known. In the case of SNRs, the main uncertainty is the availability of nearby target material. In the case of GRBs, the main uncertainty is the fraction of the extragalactic cosmic-ray population that comes from this source.

Active galaxies are complex systems with many possible sites for accelerating cosmic rays and for targets to produce neutrinos. For example, if acceleration occurs mainly at an outer termination shock in intergalactic space (38), there would be little target material available. One generic picture in which the neutrino luminosity is directly related to the contribution of the sources to extragalactic cosmic rays arises if acceleration occurs in the jets of AGN (or GRBs) (39, 40). High-energy protons interact in the intense radiation fields inside the jets. In the $p\gamma \rightarrow p\pi^0$

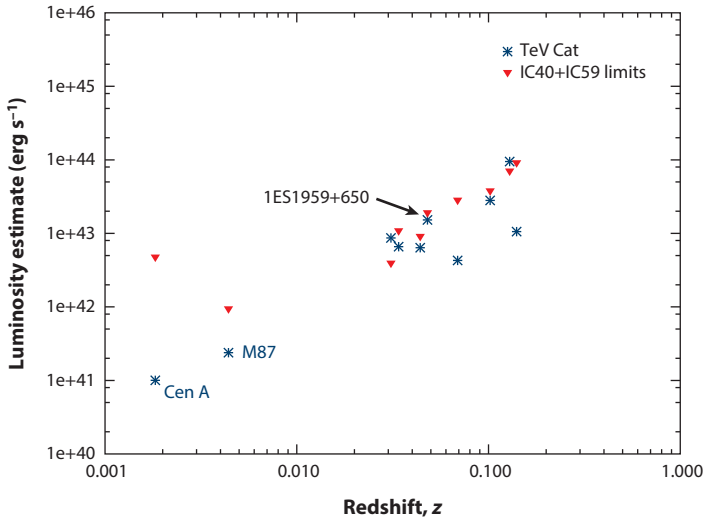

Figure 3

Limits on the neutrino flux from selected active galaxies derived from IceCube data taken during construction, when the instrument was operating with 40 and 59 strings of the total 86 instrumented strings of digital optical modules (43). These are compared with the TeV photon flux for nearby active galactic nuclei. Note that energy units are in erg, not TeV.

channel, the protons remain in the accelerator. In the $p\gamma \rightarrow n\pi^+$ channel, however, the neutrons escape and eventually decay to produce cosmic-ray protons, while the pions decay to neutrinos. The luminosity of neutrinos from photopion production is then directly related by kinematics to the cosmic-ray protons that come from decay of the escaping neutrons.

TeV γ-rays are measured from many AGN blazars (**http://tevcat.uchicago.edu/**). Although the observed γ-rays are likely to be from accelerated electrons, which radiate more efficiently than protons, the γ-ray luminosity may indicate the overall cosmic-ray luminosity and hence the possible level of neutrino production (41). In this context, we introduce **Figure 3** (42), showing IceCube upper limits (43) on the neutrino flux from nearby AGN as a function of their distance. The sources at redshifts between 0.03 and 0.2 are Northern Hemisphere blazars for which distances and intensities are listed in TeVCat (**http://tevcat.uchicago.edu/**) and for which IceCube also has upper limits. In several cases, the ν_μ limits have reached the level of the TeV photon flux. One can sum the sources shown in the figure into a diffuse flux. The result, after accounting for the distances and luminosities, is 3×10^{-9} GeV cm^{-2} s^{-1} sr^{-1}, or $\sim 10^{-8}$ GeV cm^{-2} s^{-1} sr^{-1} for all neutrino flavors. This value is at the level of the generic astrophysical neutrino flux of Equation 1. At this intensity, neutrinos from theorized cosmic-ray accelerators will cross the steeply falling atmospheric neutrino flux above an energy of ~300 TeV (**Figure 2**). The level of events observed in a cubic-kilometer neutrino detector is ~10–100 ν_μ-induced events per year. Such estimates reinforced the logic for building a cubic-kilometer neutrino detector. A more detailed description of the theoretical estimates can be found in Reference 44.

3. NEUTRINO ASTRONOMY I

The IceCube neutrino detector (**Figure 1**) consists of 5,160 digital optical modules (DOMs) viewing a cubic kilometer of clear ice between 1,450 and 2,450 m below the surface. The depth of the detector and its projected area determine the trigger rate of ~3 kHz due to penetrating

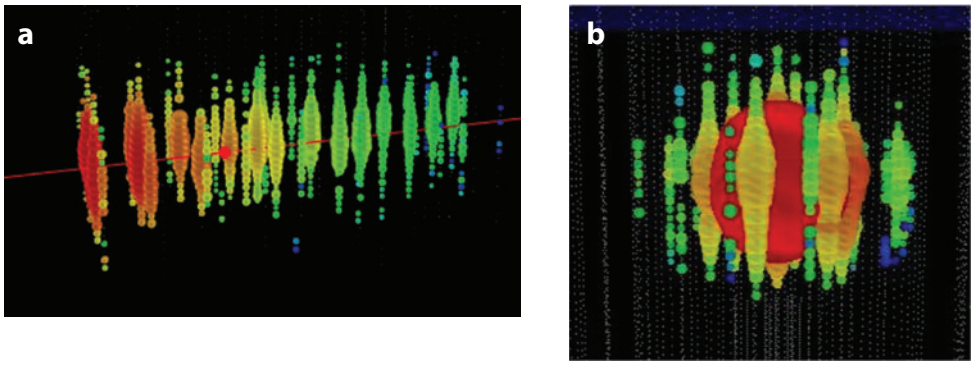

Figure 4

(*a*) A neutrino-induced muon from below the horizon crossing the detector (59). (*b*) A cascade event starting in the detector (58). The colors of the dots indicate arrival time, from early (*red*) to late (*purple*), following the rainbow. The sizes of the dots indicate the number of photons detected.

muons produced by interactions of cosmic rays in the atmosphere above. The ratio of neutrino-induced signal to atmospheric background is on the order of one per million. The neutrino rate is dominated by atmospheric neutrinos produced around the globe. The first challenge is to select a sufficiently pure sample of neutrinos, and the second is to identify the small fraction of astrophysical neutrinos.

Neutrino events may be broadly classified into two groups, tracks and cascades, which reflect the patterns of Cherenkov light emitted by the charged particles produced when the neutrinos interact. Tracks are produced by charged-current interactions of ν_μs, whereas cascades are produced by charged-current interactions of ν_es and ν_τs and neutral-current interactions of all neutrino flavors. **Figure 4** shows high-energy examples of each, discussed in Section 5 below. The ν_μ-induced muons typically travel several kilometers, whereas the characteristic length scale for the electromagnetic showers that dominate the cascade events is tens of meters. A complementary way to classify neutrino events is to distinguish events that start inside the detector from those in which the neutrino interacts outside the detector. The largest neutrino sample consists of ν_μ-induced muons entering the detector from zenith angles too large to be atmospheric muons ($\theta \geq 85°$). The rate of such events in the full IceCube detector is ~100 per day or more, depending on how the threshold for the analysis is set. The mean energy of this sample, dominated by atmospheric neutrinos, is ~1 TeV, of which only a fraction is deposited in the detector.

The starting event sample includes both tracklike and cascade events. At 2 PeV, the mean decay length of a τ lepton is comparable to the 125-m spacing between the strings of IceCube. Somewhere in the PeV range it should be possible to identify a ν_τ by its characteristic double-bang signature (45). Such an event has not yet been identified. For $E_\nu < 1$ PeV, the interaction of a ν_τ in IceCube will look much like that of a ν_e.

Reconstruction of events depends on accurate timing (<3 ns) and on the ability to measure the amount of Cherenkov light generated along the tracks of charged particles produced by the neutrino interactions. Basically, the arrival time of photons at the DOMs determines the trajectory, and the amount of light is a proxy for the deposited energy. The number of photons produced per unit path length and their distribution in wavelength are well-known quantities (46, section 30.7). An understanding of the properties of the ice (47) is crucial to relate light generated to light observed in the DOM as a function of distance and orientation relative to the emission point. Reconstruction of tracks in ice has been well studied (48). For typical kilometer tracks, the

angular resolution is better than 1°. Reconstruction of cascade events is a topic of current study at IceCube (49). Determining the deposited energy from the observed light pool is, in principle, straightforward once the vertex is located by symmetry (modulo ice properties). Angular resolution is significantly poorer than for tracks. In the large cascades studied by detailed simulations on an event-by-event basis, it is possible to determine the directions to within 15° on the basis of the shapes of the waveforms, which reflect the directionality of the cascade electrons.

4. THE FIRST KILOMETER-SCALE NEUTRINO DETECTOR

Before the first string of IceCube was deployed in January 2005, considerable effort went into designing the hot water drilling system and developing the design and assembly procedure for the DOMs. The first working season at the South Pole was 2003–2004, when major components of the drill system were shipped in and test tanks were set up for IceTop, the surface array of IceCube.

Optical modules consist of a 10-inch Hamamatsu photomultiplier (50), a main computer board, and a board with 12 light-emitting diodes for calibration, all enclosed in a watertight glass sphere. The sphere consists of two hemispherical sections, partially evacuated and sealed, with a single penetrator connecting to an external cable. DOMs were assembled at three sites: Madison, Wisconsin; Stockholm/Uppsala, Sweden; and DESY–Zeuthen, Germany.

The drilling system consisted of a number of components, starting with fuel tanks and generators followed by sets of hot water heaters, high-pressure pumps, and the drill control center, arranged in a series of buildings termed the drill camp. The drill camp was excavated from its storage location at the beginning of each austral summer, starting in late October, and relocated to the center of the drilling area for the season. Start-up included establishing a working reservoir (Rodriguez well) for the hot water drilling system. Water was recycled from the high-pressure pumps through an insulated surface hose with a reach of 300 m into a single 3-km-long, 10-cm-diameter drilling hose that moved down at a rate of 2 to 3 m min^{-1}. As drilling proceeded, water was brought back to the surface system through a return hose from the hole. Hot water continued to flow through the system as the drill hose was rewound so as to finish with a water-filled cylinder 2.5 km deep by 60 cm in diameter. The standard time for preparing a hole was 36 h.

Optical modules were staged in a tower structure adjacent to the drill tower so that deployment could begin soon after drilling was complete. The use of two systems allowed drilling and deployment to proceed in leapfrog fashion (**Figure 5**). During deployment, the drill tower was used to carry the main cable. DOMs were connected to breakouts on the cable as it descended into the hole. Two IceTop tanks, each instrumented with two DOMs, were deployed 25 m from the top of each hole. After drilling procedures were established, up to 20 strings could be deployed in a season (**Table 1**).

Data-acquisition programs running on the DOMs process photomultiplier tube (PMT) output to provide time-stamped waveforms (51). Timing at the nanosecond level is achieved through automated synchronization of a global clock distributed through kilometer-length copper wires. Surface cables bring signals from the DOMs to computers in the IceCube Lab (ICL), an elevated building in the center of the array. The computers process the DOM signals to form triggers and preliminary reconstructions of events. Events are filtered and a subset selected for transmission by satellite to the north.

5. ATMOSPHERIC MUONS AND NEUTRINOS

Muons and neutrinos from decays of mesons produced by cosmic-ray interactions in the atmosphere are the background in the search for neutrinos of extraterrestrial origin. The 3-kHz trigger

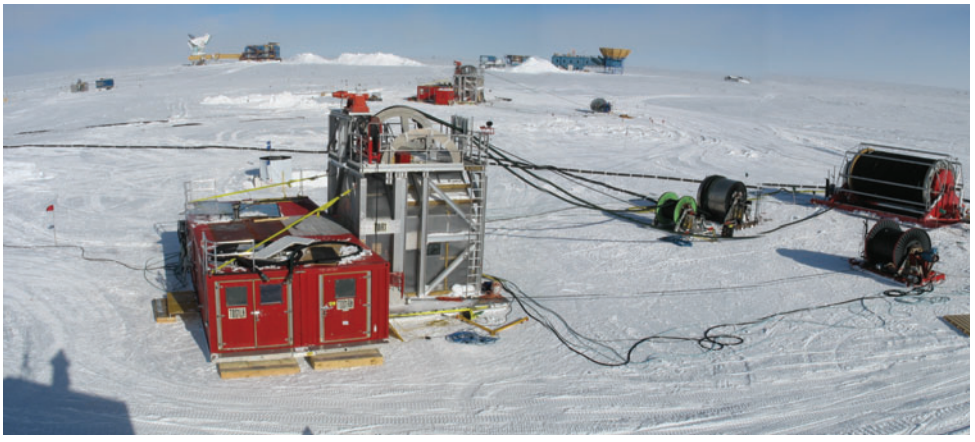

Figure 5

Photo of the drilling operation at the South Pole. The tower in the foreground is being used for drilling, while a string of digital optical modules is being deployed at the more distant tower. The South Pole Telescope (*left*) and the Martin A. Pomerantz Observatory (*right*) are visible on the horizon.

rate of IceCube is dominated by atmospheric muons from decays of pions and kaons produced in the atmosphere above the detector. The distribution peaks near the zenith and decreases with increasing angle as the muon energy required to reach the deep detector increases. Most atmospheric muons are easily identified as entering tracks from above and are rejected. Because of the large ratio of muons to neutrinos, however, misreconstructed atmospheric muons remain an important source of background for all searches.

Measurement of the spectrum of atmospheric neutrinos is an important benchmark for a neutrino telescope. The spectrum of atmospheric ν_μ has been measured by unfolding the measured rate and energy deposition of neutrino-induced muons entering the detector from below the horizon (**Figure 2**) (32). More challenging is the measurement of the flux of atmospheric ν_es. This has been done by making use of DeepCore, the more densely instrumented subarray in the deep center of IceCube, to identify contained cascade events. The known spectrum of ν_μs is used to calculate the contribution of neutral-current interactions to the observed rate of cascades. Subtracting the neutral-current contribution leads to the measurement of the spectrum of atmospheric ν_es from 100 GeV to 10 TeV (**Figure 2**) (34).

In general, atmospheric neutrinos are indistinguishable from astrophysical neutrinos. An important exception occurs in the case of ν_μs from above when the neutrino energy is sufficiently

Table 1 IceCube deployment by season (cumulative)

Season	Strings	IceTop stations
2004–2005	1	4
2005–2006	9	16
2006–2007	22	26
2007–2008	40	40
2008–2009	59	59
2009–2010	79	73
2010–2011	86	81

high and the zenith angle sufficiently small that the muon produced in the same decay as the neutrino is guaranteed to reach the detector (52). In this case, the atmospheric neutrino provides its own self-veto. By use of a Monte Carlo simulation, the atmospheric neutrino passing rate can be evaluated more generally by including other high-energy muons produced in the same cosmic-ray shower as the neutrino. In this way, the method can be extended to ν_es. In practice, the passing rate is significantly reduced for zenith angles $\theta < 70°$ and $E_\nu > 100$ TeV.

The spectrum of atmospheric neutrinos becomes one power steeper than the spectrum of primary nucleons at high energy as the competition between interaction and decay of pions and kaons increasingly suppresses their decay. For the dominant kaon channel, the characteristic energy for the steepening is $E_\nu \sim 1\,\mathrm{TeV}/\cos\theta$. A further steepening occurs above 100 TeV at the knee in the primary spectrum. Astrophysical neutrinos should reflect the cosmic-ray spectrum in the source and are therefore expected to have a significantly harder spectrum than that of atmospheric neutrinos. Establishing an astrophysical signal above the steep atmospheric background requires an evaluation of the atmospheric neutrino spectrum around 100 TeV and above.

Although there is some uncertainty associated with the composition through the knee region (53), the major uncertainty in the spectrum of atmospheric neutrinos at high energy is the level of charm production. The short-lived charmed hadrons preferentially decay up to a characteristic energy of 10^7 GeV, producing prompt muons and neutrinos with the same spectrum as their parent cosmic rays. This prompt flux of leptons has not yet been measured. Existing limits (54, 55) allow a factor of two or three around the level predicted by a standard calculation (37), after correction for steepening at the knee. For reasonable assumptions, the charm contribution is expected to dominate the conventional spectrum above ~10 TeV for ν_es, above ~100 TeV for ν_μs, and above ~1 PeV for muons (56).

The expected hardening in the spectrum of atmospheric neutrinos due to prompt neutrinos is partially degenerate with a hard astrophysical component. However, the spectrum of astrophysical neutrinos should reflect the spectrum of cosmic rays at their sources, which is expected to be harder than the spectrum of cosmic rays arriving at Earth. It should eventually be possible with IceCube to measure the charm contribution by requiring a consistent interpretation of neutrino flavors and muons for which there is no astrophysical component. An additional signature of atmospheric charm is the absence of seasonal variations for this component (57).

6. DISCOVERY OF COSMIC NEUTRINOS

The generation of underground neutrino detectors preceding construction of AMANDA searched for cosmic neutrinos without success and established an upper limit on their flux, assuming an E^{-2} energy dependence (29):

$$E_\nu^2 \frac{\mathrm{d}N}{\mathrm{d}E_\nu} \leq 5 \times 10^{-6}\,\mathrm{GeV\,cm^{-2}\,s^{-1}\,sr^{-1}}. \qquad 2.$$

Operating for almost one decade, AMANDA improved this limit by two orders of magnitude. With data taken during its construction, IceCube's sensitivity rapidly approached the theoretical flux estimates for candidate sources of cosmic rays, such as SNRs, GRBs, and with a larger uncertainty, AGN (**Figure 2**). With its completion, IceCube also positioned itself to observe the much-anticipated cosmogenic neutrinos, with some estimates predicting as many as two events per year (10).

Cosmogenic neutrinos were the target of a dedicated search using IceCube data collected between May 2010 and May 2012. Two events were found (58). However, their energies, rather than ~EeV, as expected for cosmogenic neutrinos, are just above 1 PeV. These events are particle

showers initiated by neutrinos interacting inside the instrumented detector volume. Their light pool of roughly 100,000 photoelectrons extends over more than 500 m (**Figure 4*b***). With no evidence of a muon track, both are most likely initiated by ν_es or ν_τs.

Before this serendipitous discovery, neutrino searches had almost exclusively focused on ν_μs that interact primarily outside the detector to produce kilometer-long muon tracks passing through the instrumented volume. This approach maximizes the event rate by enlarging the target volume, but it is necessary to use the Earth as a filter to remove the huge background flux of muons produced by cosmic-ray interactions in the atmosphere. This approach limits the neutrino view to a single flavor and half the sky. Inspired by the observation of the two PeV events, a filter was designed to identify high-energy neutrinos interacting inside the detector. It divides the instrumented volume of ice into an outer veto shield and a 420-MT inner fiducial volume. The separation between veto and signal regions was optimized to reduce the background of atmospheric muons and neutrinos to a handful of events per year while keeping 98% of the signal. The background of atmospheric muon punch-through was determined experimentally by measuring the rate at which muons tagged in the veto region passed an inner veto region of similar size. The great advantage of specializing to neutrinos interacting inside the instrumented volume of ice is that the detector functions as a total absorption calorimeter measuring deposited energy with 10–15% resolution. Also, neutrinos from all directions in the sky, including both muon tracks produced in ν_μ charged-current interactions and secondary showers produced by neutrinos of all flavors, can be identified.

Analyzing the data covering the same time period as the cosmogenic neutrino search, 28 candidate neutrino events were identified with in-detector deposited energies between 30 and 1,140 TeV (20). Most of the events, including the two previously discovered PeV events, come from the southern sky. Some of these events have sufficiently high energy and small zenith angle so that, if they were produced in the atmosphere, they would probably have been accompanied by muons and excluded from the data sample.

Of the 28 events, 21 are showers with no evidence of a muon track and with energies measured to better than 15%, although their directions are determined to 10–15° only. The remaining 7 events are muon tracks, which do allow for subdegree angular reconstruction; however, only a lower limit on their energy can be established because of the unknown fraction carried away by the exiting muon. Furthermore, the lower-energy muon-like events from above include four that start near the detector boundary and are consistent with the expected background of atmospheric muons. The expected background is $10.6^{+5.0}_{-3.6}$ events, which has comparable contributions from atmospheric muons and atmospheric neutrinos. The sample of 28 events represents an excess of more than 4σ above background.

Figure 6 shows the energy and zenith-angle dependence of the 28 events. There is a significant excess of events above 100 TeV compared with the background expectation. Both the energy and zenith-angle dependence observed are consistent with what is expected for a flux of neutrinos produced by cosmic-ray accelerators. The flavor composition of the flux is, after corrections for the acceptances of the detector to the different flavors, consistent with 1:1:1, as anticipated for a flux originating in cosmic sources.

The large errors on the background are associated with the possible presence of a neutrino component originating from the production and prompt leptonic decays of charmed particles in the atmosphere. Such a flux has not been observed so far. Although its energy and zenith-angle dependence are known, its normalization is not; see **Figure 2** for one attempt at calculating the flux of charm origin. Neither the energy nor the zenith-angle dependence of the 28 events observed can be described by a charm flux, and in any case, fewer than 3.4 events are allowed at the 1σ level by the present upper limit on a charm component of the atmospheric flux set by IceCube itself (55).

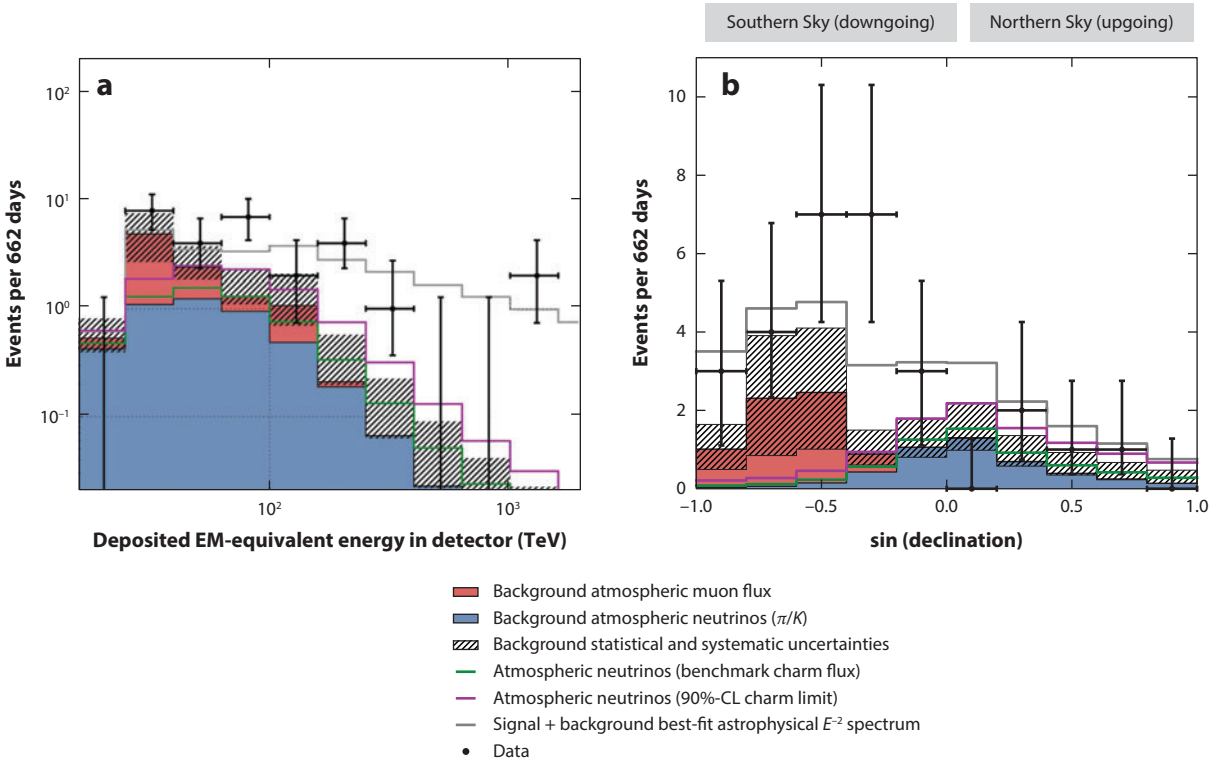

Figure 6

Distribution of (*a*) the deposited energies and (*b*) declination angles of the observed events compared with model predictions. Energies plotted are in-detector visible energies, which are lower limits on the neutrino energy. Note that deposited energy spectra are always harder than the spectra of the neutrinos that produced them because the neutrino cross section increases with energy. The expected rate of atmospheric neutrinos is based on Northern Hemisphere muon neutrino observations. The estimated distribution of the background from atmospheric muons is shown in red. Due to lack of statistics from data far above the cut threshold, the shape of the distributions from muons in this figure has been determined using Monte Carlo simulations, with total rate normalized to the estimate obtained from the in-data control sample. Combined statistical and systematic uncertainties on the sum of backgrounds are shown as a hatched area. The gray line shows the best-fit E^{-2} astrophysical spectrum with all-flavor normalization (1:1:1) of Equation 3 and a spectral cutoff of 2 PeV. Abbreviation: EM, electromagnetic. Modified from Reference 20 with permission.

Fitting the data to a superposition of extraterrestrial neutrinos on an atmospheric background yields a cosmic-neutrino flux of

$$E_\nu^2 \frac{\mathrm{d}N}{\mathrm{d}E_\nu} = 3 \times 10^{-8}\,\mathrm{GeV\,cm^{-2}\,s^{-1}\,sr^{-1}} \qquad 3.$$

for the sum of the three neutrino flavors. As discussed in Section 2, this is the level of flux anticipated for neutrinos accompanying the observed cosmic rays.

So, where do the neutrinos come from? A map of their arrival directions is shown in **Figure 7**. A test statistic, $\mathrm{TS} = 2 \times \log L/L_0$, was used, where L is the signal-plus-background maximized likelihood and L_0 is the background-only likelihood obtained by scrambling the data. No significant spot on the sky was found when the data were compared with randomized pseudoexperiments. A repeated analysis only for showers showed a hot spot at a right ascension of 281° and a declination of 23° close to the Galactic center. After correcting for trials, the probability corresponding to its TS is 8%. Searches were also made for clustering of the events in time and for a possible

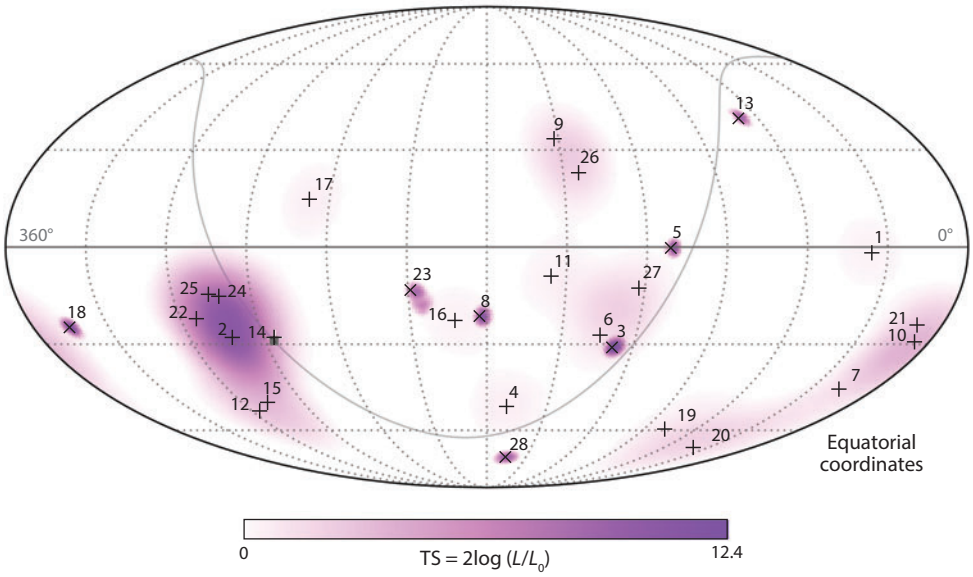

Figure 7

Sky map in equatorial coordinates of the test statistic (TS) that measures the probability of clustering among the 28 events. The most significant cluster consists of five events—all showers and including the second-highest-energy event in the sample—with a final significance of only 8%. The Galactic plane is shown as a gray line, and the Galactic center appears as a filled gray square. Best-fit locations of individual events are indicated with vertical crosses (+) for showers and angled crosses (x) for muon tracks. Modified from Reference 20.

correlation with the times of observed GRBs. No statistically significant correlation was found. Fortunately, more data are already available, and the analysis, performed blind, can be optimized for searches of future data samples.

7. NEUTRINO ASTRONOMY II

During construction, IceCube collected more than 100,000 ν_μs from the Northern Hemisphere, detected by their secondary, upgoing muon tracks originating in neutrino interactions inside or near the detector. Above neutrino energies of tens of TeV, where potential sources may dominate the steeply falling atmospheric neutrino background, these tracks are reconstructed to better than 0.5°; at these energies neutrino and muon directions are aligned. The muons lose energy predominantly by catastrophic interactions in the ice, and the measured dE/dx of the muon inside the detector can be used as a proxy for the neutrino energy. A straightforward way to search for sources of neutrinos is to look for clustering of events in arrival direction; the energy of the events in a cluster can subsequently be used to further separate very high energy cosmic neutrinos from atmospheric background. As discussed in the previous section, at energies above 300 TeV, atmospheric neutrino events are very rare and energy is sufficient to establish an extraterrestrial source, even in the Southern Hemisphere.

The status of the point source search is summarized in the 3-year sky map (60) obtained when IceCube took data between April 2008 and May 2011 with partial configurations of 40, 59, and 79 out of 86 strings when completed (**Figure 8**). As in **Figure 7**, the color scheme shows at each

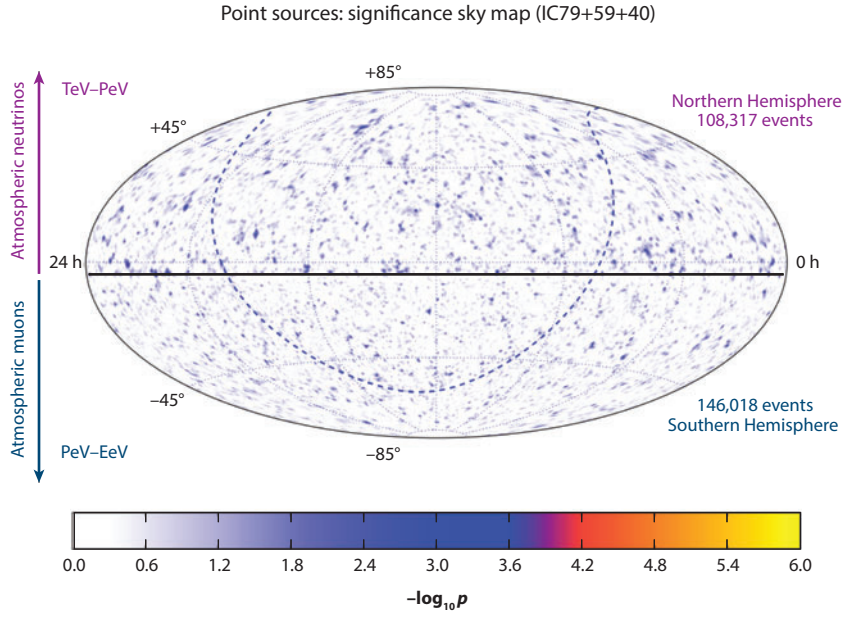

Figure 8

Pretrial significance sky map in equatorial coordinates (J2000) of the all-sky point source scan for the combined IC79+IC59+IC40 data sample (60). The dashed line indicates the Galactic plane. Modified from Reference 60.

location in the sky the probability of a source based on $\mathrm{TS} = 2 \times \log L/L_0$, where, in this case, L is the likelihood that a source with spectral index γ produces a signal with the significance shown. The likelihood of background L_0 is evaluated using the data, which are dominated by background.

For the detailed definition of the probability distribution functions, we refer the reader to Reference 60. In brief, for a source location $\boldsymbol{x_s}$, each event is assigned a source probability density corresponding to the probability of the event belonging to a source at $\boldsymbol{x_s}$. The source probability density is the product of a spatial density function describing the potential of an event reconstructed with direction $\boldsymbol{x_i}$ to have true direction $\boldsymbol{x_s}$ and the probability of observing reconstructed muon energy E_i given the source spectral index. The source is assumed to emit neutrinos according to an $E^{-\gamma}$ power law energy spectrum.

To evaluate the posttrial probability, also known as the look-elsewhere effect, one performs pseudoexperiments in which the data are randomized to determine the significance of a possible excess. This unbinned likelihood analysis results in sensitivity (upper limit in the absence of an excess) and discovery potential as a function of zenith angle (**Figure 9**). Neutrino limits on northern sources still exceed expectations by a factor of a few, but IceCube point source analysis is approaching the sensitivity to reveal sources associated with the cosmic-neutrino flux in **Figure 7**.

Promising targets include the hard-spectrum sources observed by the MILAGRO γ-ray telescope at tens of TeV with a differential slope $\gamma \simeq 2$. Such sources produce a neutrino flux on the order of $E_\nu^2(\mathrm{d}N/\mathrm{d}E_\nu) \simeq 10^{-12}$ TeV cm^{-2} s^{-1}, assuming that the observed γ-rays are of pionic origin (62). This is definitely the case for γ-ray production by cosmic rays in molecular clouds. At this level, only about one event per year is expected in IceCube. However, such a low rate may be sufficient to produce a statistically significant signal after several years because the atmospheric

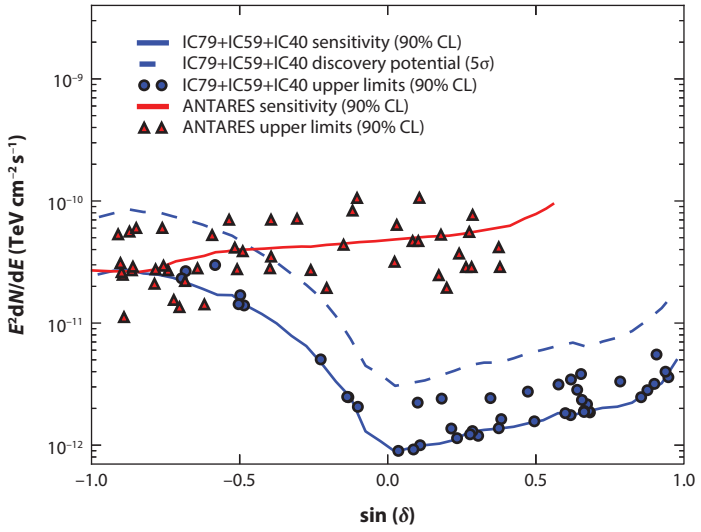

Figure 9

Muon neutrino and antineutrino flux 90%-CL upper limits and sensitivities for an E^{-2} spectrum (60) and the published limits of ANTARES (61). The different likelihood function and method to derive upper limits used by ANTARES may account for differences in the limits from the two experiments at the level of 20%. The points show the actual upper limits for a list of selected point sources. Modified from Reference 60.

flux within a ∼0.5° bin defined by the resolution is smaller yet, especially at the higher energies. Therefore, not only the slope of the energy spectrum but also how high a source extends in energy is critical. Sources of the still-unidentified "PeVatrons" that accelerate the highest-energy Galactic cosmic rays to the knee would be expected to produce secondary pionic γ-rays and neutrinos of several hundred TeV, provided that their environment is suitable for pion production.

GRBs constitute a special class of point sources because they cluster in both space and time. A powerful model-independent analysis method has been developed to search for neutrinos coincident in time (up to 1,000 s) and direction with GRB flares observed by satellites, most prominently *Fermi* and *Swift*. Data taken with the 40- and 59-string configurations led to an upper limit on the GRB flux that is a factor of four below the predictions (63). This result implies either that GRBs alone cannot account for the flux of extragalactic cosmic rays or that the efficiency of neutrino production is much lower than has been predicted. Scanning a wider time window, an event with 109 TeV deposited energy and angular resolution within 0.2° of a *Swift* GRB was found to have the most significant correlation, even though it was 14 h before the GRB. Subsequent analysis showed that the event had hits in IceTop, marking it as a cosmic-ray background event and at the same time illustrating the sparseness of the background for the GRB search with ν_μ-induced muons. With GRBs on probation, the stock rises for the alternative speculation that associates supermassive black holes at the centers of galaxies with the unaccounted-for cosmic-ray accelerators. Suggestions to reduce the GRB neutrino flux prediction (64) will be confronted with rapidly improving limits from a completed detector.

8. COSMIC RAYS

The high-energy cosmic-ray spectrum is related to neutrino astrophysics with IceCube in two ways. At Earth, it produces the atmospheric muons and neutrinos that are the background for

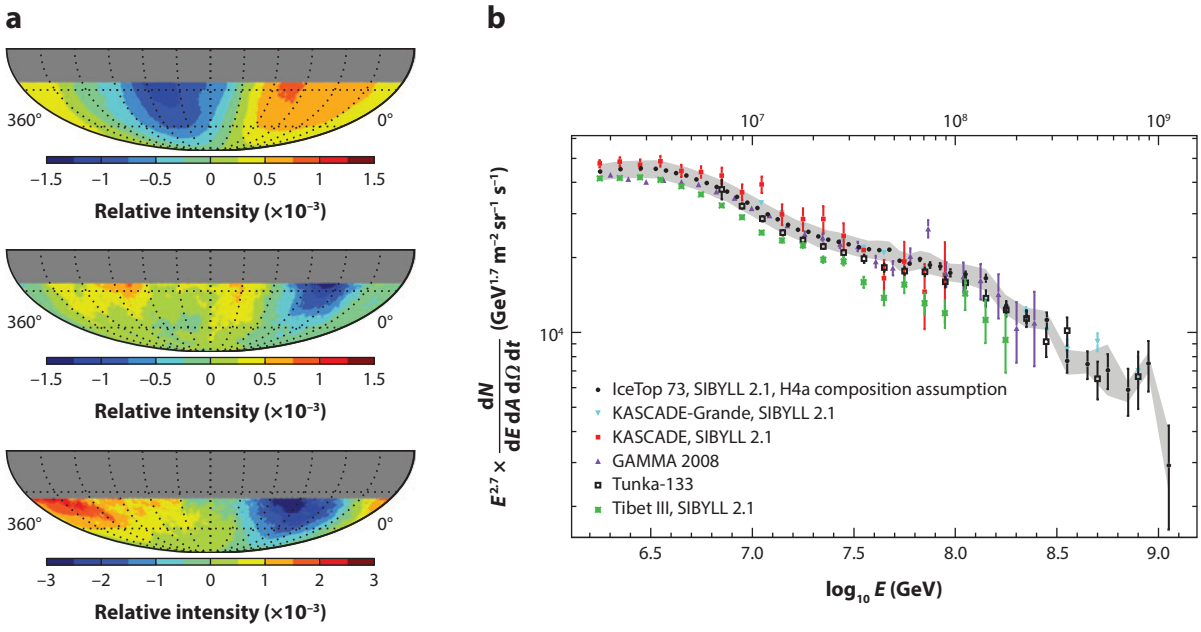

Figure 10

(*a*) Maps of cosmic-ray intensity measured with IceCube with (*top to bottom*) mean energies of 20 (65), 400 (66), and 2,000 TeV (67). (*b*) Primary cosmic-ray spectrum measured with IceCube. The black points represent the energy spectrum so far measured with IceTop. The shaded gray band represents the largest contribution to the systematic uncertainty in the spectrum from IceTop alone. Panel *b* modified from Reference 72.

astrophysical neutrinos. In the cosmos, in or near their sources and during propagation, cosmic rays interact to produce secondary particles, including γ-rays and neutrinos.

Two aspects of the cosmic-ray spectrum at Earth are being measured by IceCube. One is the anisotropy in the arrival directions of the cosmic rays in the energy range from 20 TeV to 2 PeV (**Figure 10*a***). The lower-energy measurements [~20 (65) and ~400 TeV (66)] are made using penetrating muons reconstructed in the deep array of IceCube. The high-energy plot (~2 PeV) is made with the IceTop air shower array on the surface (67). These are the first measurements of the cosmic-ray anisotropy in the southern sky and complete the view of cosmic-ray arrival directions in this energy range observed by detectors in the north (68, 69). The data here are smoothed on a 20° angular scale. Anisotropies have also been measured on a smaller scale (70). A noteworthy feature of the large-scale anisotropy in **Figure 10** is that its phase changes between 20 and 400 TeV and then persists as energy increases further. The amplitude increases as well, going to 2 PeV.

With its surface component, IceTop (71), IceCube is a three-dimensional array for cosmic-ray physics. The main goal is to measure the spectrum and composition of the cosmic rays from 300 TeV to above 1 EeV. **Figure 10*b*** shows the energy spectrum measured so far with IceTop (72) in comparison with several other measurements made in the past decade (73–77). The fine resolution obtained with IceTop is in part due to the high altitude at the South Pole, which allows the showers to be measured near their maximum, reducing shower-to-shower fluctuations. As a consequence, the measurement is able to reveal deviations from smooth power law behavior with a high degree of resolution. In addition to the steepening of the spectrum in the well-known knee

region above 3 PeV, there is a structure around 100 PeV where the spectrum first hardens, starting at 20 PeV, and then steepens above 140 PeV.

The largest contribution to the systematic uncertainty in the spectrum from IceTop alone (**Figure 10**) is from uncertainty in the assumption about primary composition that is made to obtain the energy spectrum. Information about the composition can be obtained using the full three-dimensional capability of IceCube to measure the energy deposition in the deep detector, as well as the shower at the surface for the subset of showers with trajectories that pass through both parts of the detector. The ratio of shower size at the surface to energy deposited by the muon bundle in the deep ice is sensitive to primary composition because heavy nuclei produce more muons at a given energy than do light nuclei. A preliminary analysis (78) uses a neutral network to unfold energy spectrum and composition. The energy spectrum obtained agrees well with that measured by IceTop alone, whereas the proportion of heavy nuclei increases from 1 to 300 PeV.

9. SEARCH FOR DARK MATTER

IceCube searches indirectly for dark matter by looking for neutrinos from concentrations of weakly interacting massive particles (WIMPs) in the Sun (79), in the Milky Way (80, 81), and in nearby external galaxies (82). The neutrinos are secondary products of annihilation of pairs of WIMPs into Standard Model particles, which include decays to neutrinos. In the case of annihilation in the Sun or the Earth, only prompt decays allow production of neutrinos.

IceCube is most sensitive to WIMPs with significant spin-dependent cross sections with protons. These would lead to strong concentrations of WIMPs in the Sun, a nearby and readily identifiable source. The signal would simply be an excess of neutrinos from the direction of the Sun over the atmospheric neutrino background in the same angular window. There would be no alternative astrophysical explanation of such a signal. In most WIMP scenarios, the cross sections for WIMP capture ($\sigma_{\chi,p}$) and for WIMP annihilation ($\sigma_{\chi,\chi}$) are sufficiently large for an equilibrium between capture and annihilation to be achieved within the age of the solar system (83). In this case, limits on neutrinos from the Sun can be expressed in terms of the capture cross section, $\sigma_{\chi,p}$. If equilibrium is not reached, weaker limits can still be calculated.

Figure 11 shows the current IceCube limits (79). Also shown is a sampling of the WIMP parameter space that is not ruled out by other experiments. IceCube has produced the most stringent limits on the cross section for spin-dependent interactions of dark matter particles with ordinary matter.

A WIMP may interact with ordinary nuclei by spin-independent (e.g., Higgs boson exchange) and spin-dependent (e.g., Z boson exchange) interactions. The first mechanism favors direct detection experiments (84) because the WIMP interacts coherently, resulting in an increase in sensitivity proportional to the square of the atomic number of the detector material. The latter favors indirect experiments in which the rates are dominated by spin-dependent interactions with protons. In the case of the Sun, the WIMPs have accumulated over solar timescales, sampling the dark matter throughout the galaxy and averaging out any structure in the halo that theory may not have accounted for. Within the context of supersymmetry, direct and indirect experiments are complementary.

Quantitative interpretation of the IceCube limits is complicated, depending on detailed analysis of capture rates and annihilation channels. The analysis uses DarkSUSY (83), which builds on the classic calculations by Gould (85 and references therein) for capture and annihilation rates. The neutrino spectrum from annihilation of pairs of WIMPs depends on the dominant channel for coupling to Standard Model particles. The neutrino spectrum at production is also modified by subsequent interactions and oscillations of neutrinos as they propagate out from the solar

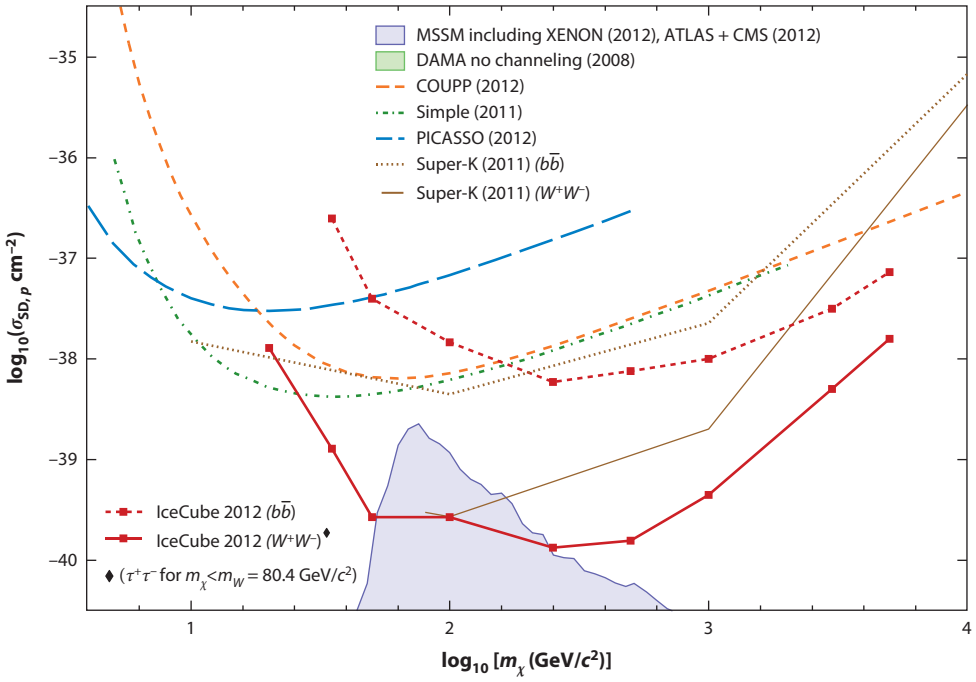

Figure 11

Upper limits at 90% CL on the spin-dependent neutralino–proton cross section, assuming that the neutrinos are produced by $b\bar{b}$ and WW annihilation (79). Limits from the Super-Kamiokande (Super-K) and direct detection experiments are shown for comparison. The shaded region represents supersymmetric models that have not been ruled out by direct experiments. Abbreviation: MSSM, minimal supersymmetric Standard Model. Modified from Reference 79.

core. Three flavor oscillations with matter effects are included (e.g., Reference 86). The range of possibilities is bracketed by calculating two extremes,

$$\chi\,\chi \rightarrow b\bar{b} \text{ (soft) and } \chi\,\chi \rightarrow W^+W^- \text{ (hard).} \qquad 4.$$

In the hard channel, $W^{\pm}$ are replaced by $\tau^{\pm}$ for $m_{\chi} < m_W$.

The IceCube limits in **Figure 11** are based on observations of ν_μ-induced muons with the nearly complete detector with 79 strings of DOMs, including for the first time the DeepCore subarray. Data were collected from May 2010 to May 2011, including the austral summer (October–March), when the Sun is above the horizon. By including events that start inside DeepCore (summer and winter), the mass range for the WIMP search could be extended down to 20 GeV, which overlaps some of the allowed region from the DAMA experiment (87). By including muons from below the horizon entering IceCube from outside (winter only because of the high background of cosmic-ray muons from above), the mass range is extended to 5 TeV.

10. IceCube AS A DISCOVERY INSTRUMENT

10.1. Neutrino Oscillations

The first IceCube oscillation analysis (88) also uses data from the 79-string detector from May 2010 to May 2011. The analysis is based entirely on ν_μ-induced muons from below the horizon. Taking

advantage of the DeepCore subarray of IceCube allowed neutrino oscillations to be observed over an energy range including the oscillation minimum around 25 GeV for propagation through the diameter of the Earth. Data were divided into two samples: muon tracks reconstructed using the entire IceCube detector ($E_\nu > 100$ GeV) and events starting in DeepCore ($20 < E_\nu < 100$ GeV). The low-energy sample consists of 719 events, whereas the high-energy sample includes 39,638 events. The high-energy sample, in which standard oscillations do not affect the rates, was used for calibration. A deficit is observed in the low-energy sample, in which ~25% more events would have been detected in the absence of oscillations. Taking account of systematic uncertainties, including ± 0.05 in the spectral index of the atmospheric neutrino flux at production, the no-oscillation hypothesis was rejected at more than 5σ. The fitted values of the oscillation parameters in a two-flavor fit are $|\Delta m^2_{32}| = 2.3^{+0.5}_{-0.6} \times 10^{-3}$ eV^2 and $\sin^2 2\theta_{23} > 0.93$. For comparison, a recent global three-flavor analysis (89) gave 2.4×10^{-3} eV^2 and 0.95, respectively, with a range of $\pm 5\%$ at 1σ and a slight dependence on the mass hierarchy. Although the measured oscillation parameters agree with previous experiments, it is important to realize that they have been measured at a characteristic energy that is higher. The measurement is therefore also sensitive to any new neutrino physics, an important consideration when the precision of the IceCube measurements will be significantly improved.

10.2. Supernovae and Solar Flares

In addition to the normal acquisition of events that reconstruct as tracks or cascades in the deep array of IceCube and as air showers in IceTop, the rates at which the PMT voltages cross the thresholds of discriminators in the DOMs are continuously monitored. A typical rate for DOMs in the deep ice is 500 Hz (including correlated afterpulses), most of which is noise. Typical rates in the high-gain DOMs of IceTop are 2–5 kHz, most of which is induced by low-energy photons, electrons, and muons entering the tanks.

A sudden increase in the total summed counting rate of the deep DOMs would signify a potential supernova explosion in the Galaxy. Supernova neutrinos of ~10 MeV interacting within a few meters of a DOM would generate enough hits to cause a sharp increase in the summed counting rate followed by a characteristic decline (90). IceCube records a dc current that tracks the time evolution of the supernova in microsecond time bins. However, the detector records the time of every photoelectron with nanosecond precision, and the binning can therefore be improved off-line, which will improve the capability to identify the deleptonization burst. The additional measurement of the rate of two-photon correlations is sensitive to the energy of the supernova neutrinos.

In IceTop, sudden changes in rates occur in response to solar events. Forbush decreases, in which the plasma from a solar flare abruptly reduces the rate of cosmic rays entering the atmosphere, are frequently detected and can be analyzed. More rare are sudden increases caused by solar energetic particles that enter the atmosphere with sufficient energy to generate secondary cosmic rays that reach the IceTop tanks. The event of December 13, 2006, was measured with the 16 tanks (8 stations) then in operation (91). The flare of May 17, 2012, is currently being analyzed.

10.3. IceCube, The Facility

During its construction phase, IceCube demonstrated significant potential for facilitating a range of other research projects. For example, a dust logger provided measurements with millimeter precision that are valuable for event reconstruction in IceCube but that also provide a record of surface winds for more than 100,000 years (92).

During the construction of AMANDA, antennas forming the RICE detector were already deployed in some holes to expand the target volume in the search for cosmogenic neutrinos (93). An acoustic test setup of receivers in the upper portion of four IceCube holes was deployed in 2007 to explore the acoustic technique for detecting ultrahigh-energy neutrinos. A retrievable transmitter (pinger) was submerged briefly in several newly prepared holes at various depths and distances from the receivers to measure the attenuation of sound in ice. The attenuation length of 300 m is significantly shorter than had been expected (94). The Askaryan Radio Array (ARA) (95) plans to take advantage of the kilometer-scale attenuation for radio signals in ice to construct a detector with a 200-km^2 effective area. That effective area should be sufficient to determine the level of production of cosmogenic neutrinos, which at present is highly uncertain (10). The initially deployed ARA detectors send data to computers housed in the ICL for staging and transmission to the north.

The DM-Ice experiment (96) proposes to repeat the DAMA experiment in the quiet environment of the Antarctic ice. An interesting feature of the observation is that the seasonal modulation of the muon rate has the opposite phase relative to the motion of the Earth through the gas of dark matter as compared with a detector in the Northern Hemisphere. A test detector to explore the noise environment for DM-Ice was deployed at the bottom of an IceCube string in December 2010. Its computers and data transmission are also hosted in the ICL.

The enhancement of the low-energy capabilities of IceCube provided by the DeepCore subarray led to the PINGU proposal (97) to deploy an additional 40 strings within the existing DeepCore detector, which would lower the threshold to below 5 GeV (<25-m muon track length in ice). In this energy range, matter effects in the Earth lead to resonant oscillations of $\nu_\mu \leftrightarrow \nu_e$ ($\bar{\nu}_\mu \leftrightarrow \bar{\nu}_e$) for normal (inverted) hierarchy (98) that depend on zenith angle. The fact that the neutrino cross section is larger than that for antineutrinos, coupled with the excess of ν_μ compared with $\bar{\nu}_\mu$, allow the possibility of a measurement sensitive to the neutrino mass hierarchy on a relatively short timescale. PINGU would also have sensitivity to ν_μ disappearance, ν_τ appearance, and maximal mixing. The lower-energy threshold would also enhance the indirect searches for dark matter with IceCube, as well as the sensitivity to neutrinos from supernova explosions. In addition, there is the potential for neutrino tomography of the Earth with PINGU.

The observation of the extraterrestrial neutrinos up to the PeV range has stimulated ideas to enhance the discovery potential also in that area. One possibility is to improve the atmospheric neutrino veto by expanding the surface array (99). Expansion of the existing array with strings at larger separation is also possible in the long term.

11. OUTLOOK

Having found the first few high-energy neutrinos of extraterrestrial origin, the obvious next task for IceCube is to identify their sources. How long this will take depends on the nature of the sources. In the case of extragalactic sources, the answer depends on the number and distribution of sources (100). Because the Universe is transparent to neutrinos, if there is a large number of sources of comparable strength, then many neutrinos from random directions may be counted before there are enough to identify a single nearby source. However, if Galactic sources contribute, then identification of the sources should be possible on a well-defined timescale, as in the example discussed in Section 7.

More than 30 papers have been written suggesting possible sources for the neutrinos detected by IceCube since the two PeV events were discovered. Of these, approximately two-thirds favor an extragalactic origin, and at least one paper proposes a combination of Galactic and extragalactic sources. IceCube has a design lifetime of more than 15 years, and the detector continues to work

well. By the time this article is published, an additional 2 years of data will have been accumulated, compared with the publication in *Science* (20). An additional cascade event with ~2 PeV of energy has already been identified in the later data, although an unbroken E^{-2} power law appears unlikely. The question of the spectrum will be clarified as more data are accumulated. Rapid progress in sorting out the possible models of the sources is expected.

DISCLOSURE STATEMENT

The authors are not aware of any affiliations, memberships, funding, or financial holdings that might be perceived as affecting the objectivity of this review.

ACKNOWLEDGMENTS

We are grateful to our colleagues in the IceCube Collaboration who make the science a reality and to the many individuals and agencies involved in the construction and operation of IceCube. The operation of IceCube is supported primarily by the US National Science Foundation with substantial additional support from several national and international agencies. A list of IceCube institutions is available at **http://icecube.wisc.edu/collaboration**. A list of agencies providing support for research with IceCube is posted at **http://icecube.wisc.edu/collaboration/funding**.

LITERATURE CITED

1. Reines F, Cowan CL Jr. *Nature* 17:446 (1956)
2. Greisen K. *Annu. Rev. Nucl. Part. Sci.* 10:63 (1960)
3. Reines F. *Annu. Rev. Nucl. Part. Sci.* 10:1 (1960)
4. Markov MA. *Proc. 1960 Int. Conf. High Energy Phys.* 1:578 (1960)
5. Gaisser TK, Halzen F, Stanev T. *Phys. Rep.* 258:173 (1995); Gaisser TK, Halzen F, Stanev T. Erratum. *Phys. Rep.* 271:355 (1995); Learned JG, Mannheim K. *Annu. Rev. Nucl. Part. Sci.* 50:679 (2000); Halzen F, Hooper D. *Rep. Prog. Phys.* 65:1025 (2002); Becker J. *Phys. Rep.* 458:173 (2008); Katz UF, Spiering C. *Prog. Part. Nucl. Phys.* 67:651 (2012); Halzen F. *Nuovo Cim.* 36:N3 (2012)
6. Roberts A. *Rev. Mod. Phys.* 64:259 (1992)
7. Berezinsky VS, Zatsepin GT. *Phys. Lett. B* 28:423 (1969)
8. Greisen K. *Phys. Rev. Lett.* 16:748 (1966)
9. Zatsepin GT, Kuz'min VA. *J. Exp. Theor. Phys. Lett.* 4: 78 (1966)
10. Wdowczyk J, Tkaczyk W, Wolfendale AW. *J. Phys. A* 5:1419 (1972); Stecker FW. *Astrophys. Space Sci.* 20:47 (1973), Berezinsky VS, Smirnov AY. *Astrophys. Space Sci.* 32:461 (1975); Ahlers M, et al. *Astropart. Phys.* 34:106 (2010)
11. Zheleznykh I. *Int. J. Mod. Phys.* 21S1:1 (2006); Markov M, Zheleznykh I. *Nucl. Phys.* 27:385 (1961)
12. Babson J, et al. *Phys. Rev. D* 42:3613 (1990)
13. Balkanov VA, et al. (BAIKAL Collab.) *Nucl. Phys. B Proc. Suppl.* 118:363 (2003)
14. Aggouras G, et al. (NESTOR Collab.) *Astropart. Phys.* 23:377 (2005)
15. Aguilar JA, et al. (ANTARES Collab.) *Astropart. Phys.* 26:314 (2006)
16. Migneco E. *J. Phys. Conf. Ser.* 136:022048 (2008)
17. Karle A. *Proc. Int. Astron. Union Symp. 288* 8:84 (2012)
18. IceCube Collab. *Preliminary Design Document, v1.24.* **http://www.icecube.wisc.edu/science/publications/pdd/pdd.pdf** (2001)
19. Ahrens J, et al. (IceCube Collab.) *Astropart. Phys.* 20:507 (2004)
20. Aartsen MG, et al. (IceCube Collab.) *Science* 342:1242856 (2013)
21. Sommers P. *Astropart. Phys.* 39/40:88 (2012)
22. Baade W, Zwicky F. *Proc. Natl. Acad. Sci. USA* 20:259 (1934)

23. Ginzburg VL, Syrovatskii SI. *The Origin of Cosmic Rays*. Oxford, UK: Pergamon (1964)
24. Butt Y. *Nature* 460:701 (2009)
25. Gaisser TK. *AIP Conf. Proc.* 558:27 (2001)
26. Waxman E. *Phys. Rev. Lett.* 75:386 (1995)
27. Becker JK. *Phys. Rep.* 458:173 (2008)
28. Gonzalez-Garcia MC, Maltoni M, Rojo J. *J. High Energy Phys.* 0610:075 (2006)
29. Daum K, et al. (Frejus Collab.) *Z. Phys. C* 66:417 (1995)
30. Abbasi R, et al. (IceCube Collab.) *Phys. Rev. D* 79:102005 (2009)
31. Abbasi R, et al. (IceCube Collab.) *Astropart. Phys.* 34:48 (2010)
32. Abbasi R, et al. (IceCube Collab.) *Phys. Rev. D* 83:012001 (2011)
33. Abbasi R, et al. (IceCube Collab.) *Phys. Rev. D* 84:082001 (2011)
34. Aartsen MG, et al. (IceCube Collab.) *Phys. Rev. Lett.* 110:151105 (2013)
35. Honda M, et al. *Phys. Rev. D* 75:043006 (2007)
36. Barr GD, et al. *Phys. Rev. D* 70:023006 (2004)
37. Enberg R, Reno MH, Sarcevic I. *Phys. Rev. D* 78:043005 (2008)
38. Berezhko EG. *Astrophys. J.* 684:L69 (2008)
39. Gaisser TK. arXiv:astro-ph/9707283 (1997)
40. Ahlers M, et al. *Phys. Rev. D* 72:023001 (2005)
41. Alvarez-Muñiz J, Halzen F. *Astrophys. J.* 576:L33 (2002)
42. Gaisser TK. *EPJ Web Conf.* 53:01012 (2013)
43. Abbasi R, et al. (IceCube Collab.) *Astrophys. J.* 732:18 (2011)
44. Halzen F. *Nuovo Cim.* 036:81 (2013)
45. Learned JG, Pakvasa S. *Astropart. Phys.* 3:267 (1995)
46. Beringer J, et al. (Part. Data Group) *Phys. Rev. D* 86:010001 (2012)
47. Aartsen MG, et al. (IceCube Collab.) *Nucl. Instrum. Methods A* 711:73 (2013)
48. Ahrens J, et al. (AMANDA Collab.) *Nucl. Instrum. Methods A* 524:169 (2004)
49. Aartsen MG, et al. (IceCube Collab.) *J. Instrum.* 9:P03009 (2014)
50. Abbasi R, et al. (IceCube Collab.) *Nucl. Instrum. Methods A* 618:139 (2010)
51. Abbasi R, et al. (IceCube Collab.) *Nucl. Instrum. Methods A* 601:294 (2009)
52. Schönert S, Gaisser TK, Resconi E, Schulz O. *Phys. Rev. D* 79:043009 (2009)
53. Gaisser TK, Stanev T, Tilav S. *Front. Phys.* 8:748 (2013)
54. Aglietta M, et al. (LVD Collab.) *Phys. Rev. D* 60:112001 (1999)
55. Schukraft A. (IceCube Collab.) *Nucl. Phys. Proc. Suppl.* 237/238:266 (2013)
56. Gaisser TK. *EPJ Web Conf.* 52:09004 (2013)
57. Desiati P, Gaisser TK. *Phys. Rev. Lett.* 105:121102 (2010)
58. Aartsen MG, et al. (IceCube Collab.) *Phys. Rev. Lett.* 111:021103 (2013)
59. Aartsen MG, et al. (IceCube Collab.) *Phys. Rev. D* 89:062007 (2014)
60. Aartsen MG, et al. (IceCube Collab.) *Astrophys. J.* 779:132 (2013)
61. Adriá-Martínez S, et al. (ANTARES Collab.) *Astrophys. J. Lett.* 743:14 (2011)
62. Gonzalez-Garcia MC, Halzen F, Mohapatra S. *Astropart. Phys.* 31:437 (2009)
63. Abbasi R, et al. (IceCube Collab.) *Nature* 484:351 (2012)
64. Hummer S, Baerwald P, Winter W. *Phys. Rev. Lett.* 108:231101 (2012)
65. Abbasi R, et al. (IceCube Collab.) *Astrophys. J.* 718:L194 (2010)
66. Abbasi R, et al. (IceCube Collab.) *Astrophys. J.* 746:33 (2012)
67. Aartsen MG, et al. (IceCube Collab.) *Astrophys. J.* 765:55 (2013)
68. Abdo AA, et al. *Astrophys. J.* 698:2121 (2009)
69. Amenomori M, et al. (Tibet AS Gamma Collab.) *Astrophys. J.* 626:L29 (2005)
70. Abbasi R, et al. (IceCube Collab.) *Astrophys. J.* 740:16 (2011)
71. Abbasi R, et al. (IceCube Collab.) *Nucl. Instrum. Methods A* 700:188 (2013)
72. Aartsen MG, et al. (IceCube Collab.) *Phys. Rev. D* 88:042004 (2013)
73. Apel WD, et al. (KASCADE-Grande Collab.) *Phys. Rev. Lett.* 107:171104 (2011)
74. Antoni T, et al. (KASCADE Collab.) *Astropart. Phys.* 24:1 (2005)
75. Garyaka AP, et al. *J. Phys. G* 35:115201 (2008)

76. Berezhnev SF, et al. *Nucl. Instrum. Methods A* 692:98 (2012)
77. Amenomori M, et al. (TIBET III Collab.) *Astrophys. J.* 678:1165 (2008)
78. Aartsen MG, et al. (IceCube Collab.) *Proc. 33rd Int. Cosmic Ray Conf. Pap.* 0861
79. Aartsen MG, et al. (IceCube Collab.) *Phys. Rev. Lett.* 110:131302 (2013)
80. Abbasi R, et al. (IceCube Collab.) *Phys. Rev. D* 84:022004 (2011)
81. Abbasi R, et al. (IceCube Collab.) arXiv:1210.3557 [hep-ex] (2012)
82. Aartsen MG, et al. *Phys. Rev. D* 88:122001 (2013)
83. Gondolo P, et al. *J. Cosmol. Astropart. Phys.* 0407:008 (2004)
84. Sadoulet B. *Science* 315:61 (2007)
85. Gould A. *Astrophys. J.* 368:610 (1991)
86. Blennow M, Edsjö J, Ohlsson T. *J. Cosmol. Astropart. Phys.* 01:021 (2008)
87. Bernabei R, et al. *Int. J. Mod. Phys. D* 22:1360001 (2013)
88. Aartsen MG, et al. (IceCube Collab.) *Phys. Rev. Lett.* 111:081801 (2013)
89. Fogli GL, et al. *Phys. Rev. D* 86:013012 (2012)
90. Abbasi R, et al. (IceCube Collab.) *Astron. Astrophys.* 535:A109 (2011)
91. Abbasi R, et al. (IceCube Collab.) *Astrophys. J. Lett.* 689:65 (2008)
92. Bay RC, Rohde RA, Price PB, Bramall NE. *J. Geophys. Res.* 115:D14126 (2010)
93. Kravchenko I, et al. *Phys. Rev. D* 85:062004 (2012)
94. Abbasi R, et al. (IceCube Collab.) *Astropart. Phys.* 34:382 (2011)
95. Allison P, et al. *Astropart. Phys.* 35:457 (2012)
96. Cherwinka J, et al. *Astropart. Phys.* 35:749 (2012)
97. IceCube–PINGU Collab. arXiv:1401.2046 [physics] (2014)
98. Akhmedov EK, Razzaque S, Smirnov AY. *J. High Energy Phys.* 1302:082 (2013); Akhmedov EK, Razzaque S, Smirnov AY. Erratum. *J. High Energy Phys.* 1307:026 (2013)
99. Aartsen MG, et al. (IceCube Collab.) arXiv:1309.7010 [astro-ph] (2013)
100. Lipari P. *Phys. Rev. D* 78:083011 (2008)